Accepted Manuscript

Design, Synthesis and Evaluation of Novel Indandione Derivatives as Multi-functional Agents with Cholinesterase Inhibition, anti-β-amyloid Aggregation, Antioxidant and Neuroprotection properties against Alzheimer's Disease

Chandra Bhushan Mishra, Apra Manral, Shikha Kumari, Vikas Saini, Manisha Tiwari

PII: S0968-0896(16)30450-3
DOI: http://dx.doi.org/10.1016/j.bmc.2016.06.027
Reference: BMC 13083

To appear in: *Bioorganic & Medicinal Chemistry*

Received Date: 8 April 2016
Revised Date: 11 June 2016
Accepted Date: 13 June 2016

Please cite this article as: Mishra, C.B., Manral, A., Kumari, S., Saini, V., Tiwari, M., Design, Synthesis and Evaluation of Novel Indandione Derivatives as Multifunctional Agents with Cholinesterase Inhibition, anti-β-amyloid Aggregation, Antioxidant and Neuroprotection properties against Alzheimer's Disease, *Bioorganic & Medicinal Chemistry* (2016), doi: http://dx.doi.org/10.1016/j.bmc.2016.06.027

Design, Synthesis and Evaluation of Novel Indandione Derivatives as Multifunctional Agents with Cholinesterase Inhibition, anti-β-amyloid Aggregation, Antioxidant and Neuroprotection properties against Alzheimer's Disease

Chandra Bhushan Mishra[1], Apra Manral[1], Shikha Kumari[1], Vikas Saini[1], Manisha Tiwari *

Bio-Organic research laboratory, Dr. B. R. Ambedkar Centre for Biomedical Research, University of Delhi, Delhi 110007, India

*Correspondence

Dr. Manisha Tiwari
Dr. B. R. Ambedkar Centre for Biomedical Research, University of Delhi, Delhi 110007, India
E-mail: mtiwari07@gmail.com

1. These authors have contributed equally

Abstract

A series of novel 2-(4-(4-substituted piperazin-1-yl) benzylidene)-1H-indene-1,3(2H)-diones were designed, synthesized and appraised as multifunctional anti-Alzheimer agents. *In-vitro* studies of compounds **27-38** showed that these compounds exhibit moderate to excellent AChE, BuChE and Aβ aggregation inhibitory activity. Notably, compounds **34** and **38** appeared as most active multifunctional agents in the entire series and exhibited excellent inhibition against AChE (IC_{50}= 0.048 μM: **34**; 0.036 μM: **38**), Aβ aggregation (max %Inhibition 82.2%, IC_{50}= 9.2 μM: **34**; max % Inhibition 80.9%, IC_{50}= 10.11 μM: **38**) and displayed significant antioxidant potential in ORAC-FL assay. Both compounds also successfully diminished H_2O_2 induced oxidative stress in SH-SY5Y cells. Fascinatingly, compounds **34** and **38** showed admirable neuroprotective effects against H_2O_2 and Aβ induced toxicity in SH-SY5Y cells. Additionally, both derivatives showed no considerable toxicity in neuronal cell viability assay and represented drug likeness properties in the primarily pharmacokinetics study. All these results together, propelled out that compounds **34** and **38** might serve as promising multi-functional lead candidates for treatment of AD in the future.

1. Introduction

Alzheimer's disease (AD) is a chronic neurodegenerative disorder that assaults the central nervous system (CNS) by exerting progressive degeneration of its neurons.[1] AD is well characterized by dementia as well as cognitive impairments and currently affects over 48 million people worldwide.[2] Continuing for a long time, numerous investigations have focused on deciphering the underlying mechanism of AD and it has come in light that multiple factors like β-amyloid, acetylcholine (ACh), butyrylcholine and oxidative stress play a vital role in the progression of AD.[3] Nevertheless, upholding Ach levels through inhibition of acetylcholineesterase (AChE) is continuously deliberated as the "gold standard" therapeutic strategy for the management of AD. In support for this, four cholinesterase inhibitors (ChEls) named tacrine, rivastigmine, donepezil and galantamine have entered in the market and yet present in use (Figure 1).[4] However, the use of tacrine has been limited now because of its serious side effects such as hepatotoxicity, gastrointestinal disorders and hypotension. Other

drugs rivastigmine, donepezil and galantamine are effective, but they only target ACh rather than, acting as multifunctional agent to treat AD.

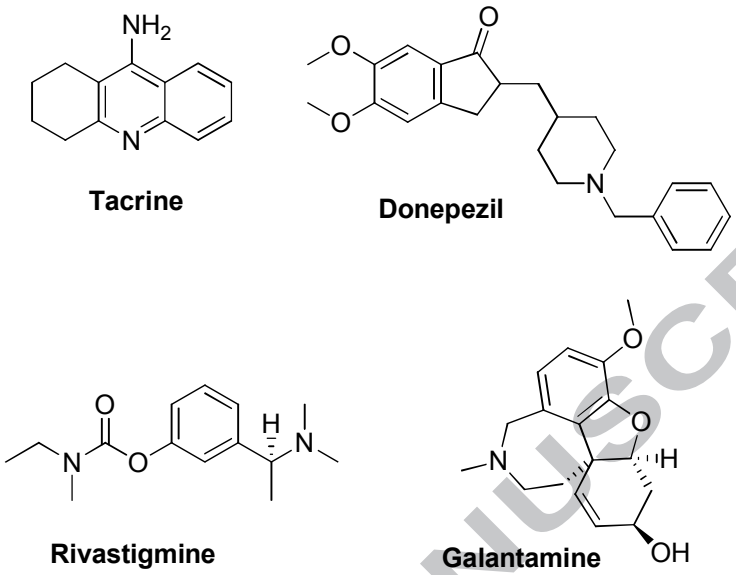

Fig 1. Chemical structures of well known Cholinesterase Inhibitors

It is well reported that accumulation of neurotoxic beta-amyloid (Aβ) peptide in the brain is a major contributing factor which leads to the progression of AD and subsequently excessive Aβ deposition exerts oxidative injury in the neuron.[5] Additionally, several studies have shown that reactive oxygen species (ROS) also play a crucial role in the development of AD because oxidative cell injury manifested by nitration, lipid peroxidation as well as nucleic acid oxidation is found in excessive levels in AD patients.[6] Collectively, Aβ fragments and neurofibrils deposition along with ROS overproduction are the main causes of neuroinflammation initiation in AD. These neuroinflammatory paradigms alter production of chemokines, cytokines and neurotoxins that precede neuronal degeneration in AD patients.[7] For this reason, neuroprotection approach is also highly beneficial and worthy strategy for AD treatment. Therefore, the combination of ChEIs, Aβ disaggregation, neuroprotection and reduction of oxidative load may produce a significant approach in AD management. By keeping this multi-factorial nature of AD in mind, researchers today are concentrated on developing new Multi-target Directed Ligands (MTLDs) to fight back against this disease.[8-9] To solve this issue, single therapeutic agent with multiple mechanism of action is inevitably required for the management of multifactorial disease

like AD. Designing of MTLDs heavily relies on the hybridization of two or more pharmacophores. By exploiting this approach various hybrid molecules have been designed and synthesized recently and fruitfully novel hybrids appeared as successful multifunctional agents to treat AD.[10-12]

We are also actively engaged to develop potent MTLDs against AD and recently we have developed piperazine/piperadine and diallyl disulfide analogs as multifunctional agent for the treatment of AD.[13-14] In this report, we have developed a novel series of 1,3 indandione derivatives to study their multifunctional potential against AD. Indandiones and their derivatives are an important class of bioactive molecules which possesses a broad spectrum biological activities such as anticoagulants, anti-microbial, analgesic, anticancer as well as antiviral activity.[15-16] On the other hand the piperazine scaffold is widely used to develop numerous biologically active agents such as antidepressants, anxiolytic, anticonvulsant, neuroprotective, antioxidant and anti-Alzheimer's.[17] To proceed with our goal, we have rationally designed a series of 2-(4-(4-substituted piperazin-1-yl)benzylidene)-1H-indene-1,3(2H)-diones which consists of indanone moiety, curcumin fragment as well as piperazine moiety inside one frame as shown in Figure 2.

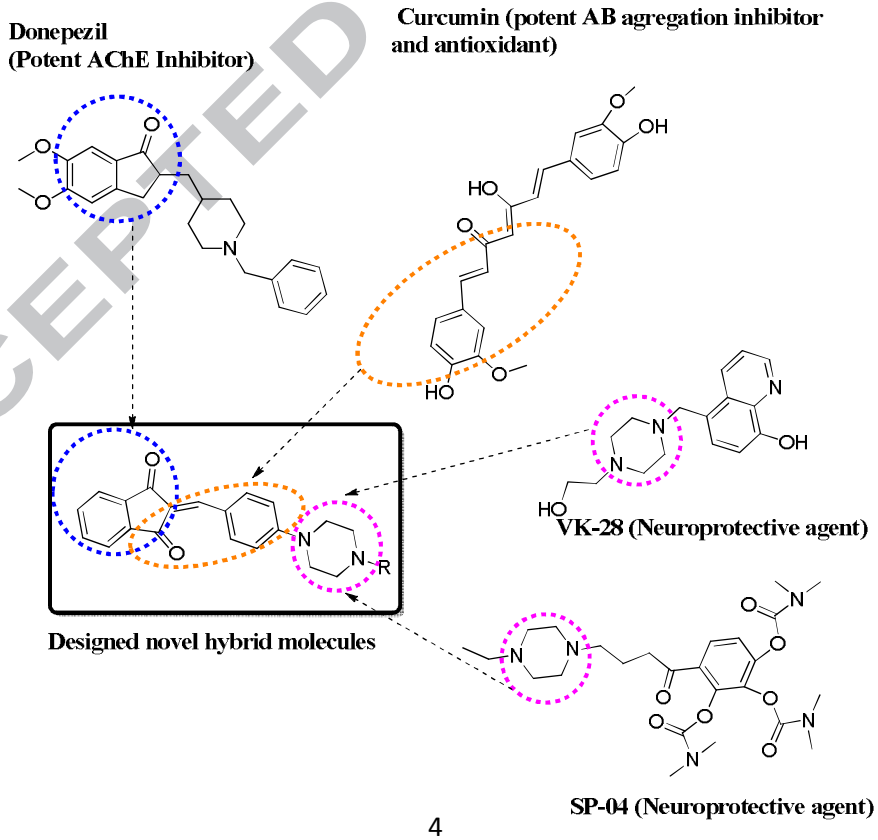

Fig 2. Designing strategy of indandione-piperazine hybrid molecules

Studies have supported that indanone moiety plays an important role in AChEs inhibition.[18] In addition to this, curcumin appeared as a potential Aβ aggregation inhibitor with potent antioxidant activity[19] and the piperazine scaffold is also used extensively to develop AChE inhibitors, neuroprotective as well as antioxidant molecules.[17] Thus, our designed molecules are endowed with necessary pharmacophoric features required for AChEs inhibition, Aβ aggregation inhibition, neuroprotective and antioxidant activity, which may warrant their multifunctional activity for AD.

2. Results and discussion

2.1. Chemistry

The synthesis of target compounds 2-(4-(4-substituted piperazin-1-yl)benzylidene)-1H-indene-1,3(2H)-dione (**27-38**) was carried out according to Scheme 1. Briefly, a mixture of substituted piperazine, 4-fluorobenzaldehyde and K_2CO_3 were heated at 130^0C in DMF for 15-24h. Thereafter, the reaction mixture was poured into ice cold water and the appeared precipitate was filtered and dried to achieve formyl derivatives **14-25**. Finally, obtained formyl derivatives **14-25** were coupled with 1,3 indandione **26** by employing Knoevenagel condensation reaction in the presence of piperidine to yield final products **27-38**. Obtained final products were purified by column chromatography using chloroform and methanol (98:2) as an eluent and fully characterized by ^{1}HNMR, ^{13}CNMR, mass spectroscopy as well as elemental analysis.

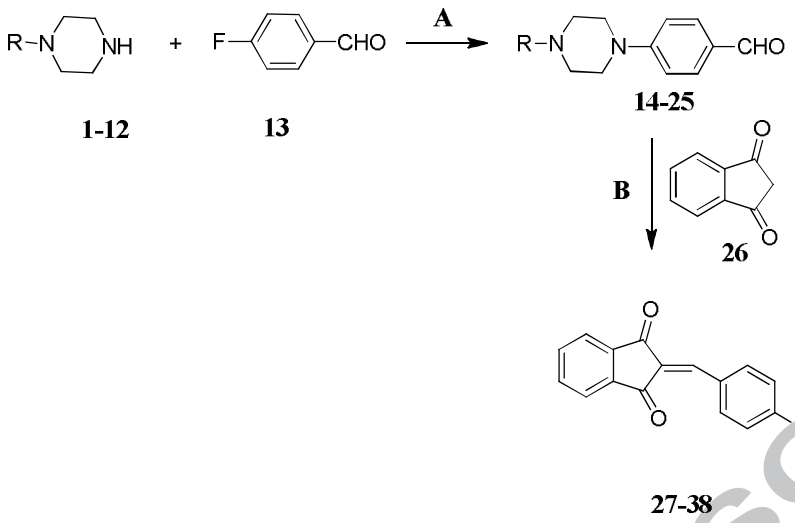

R= 1, 14, 27: Phenyl
= 2, 15, 28: *p*-fluorophenyl
= 3, 16, 29: *p*-trifluoromethylphenyl
= 4, 17, 30: *p*-chlorophenyl
= 5, 18, 31: *p*-methylphenyl
= 6, 19, 32: *o*, *p*- dimethylphenyl

R= 7, 20, 33: Benzoyl
= 8, 21, 34: Furoyl
= 9, 22, 35: Diphenylmethyl
= 10, 23, 36: Piperonyl
= 11, 24, 37: 2-pyridyl
=12, 25, 38: 2-pyrimidyl

Scheme. 1. Reagents and conditions. A; DMF, K_2CO_3, reflux; 15-24h; B. Ethanol, piperidine, reflux, 2-4h.

2.2. Cholinesterase inhibition activity and structure activity relationship (SAR)

The target compounds (**27-38**) were tested for their potential to inhibit AChE and butyrylcholinesterase (BuChE) enzymes. The IC_{50} values and selectivity index obtained for each tested compound including the reference drug donepezil, are summarized in Table 1. All tested compounds exhibits moderate to excellent inhibitory activity for both ChEls with IC_{50} values ranging from sub-micromolar to nanomolar and on the basis of these results the following structure activity relationship (SAR) was obtained. Within phenyl substituted derivatives, it was observed that the inhibitory activity against AChE was substantially improved as electron withdrawing properties of substitutent was increased and in result compound **29** (IC_{50} =

Table1. In vitro inhibition of AChE, BuChE, $A\beta_{1-42}$ aggregation and oxygen radical absorbance capacity (ORAC, Trolox equivalents) of compounds **27-38**

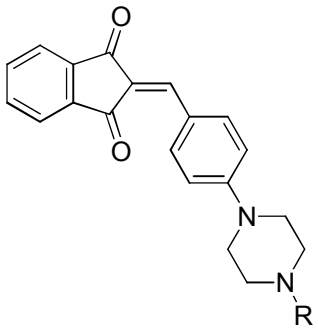

Compound	where 'R'	IC_{50} ± S.D (μM)		SI[c] (BuChE/ AChE)	$A\beta_{1-42}$ aggregation inhibition (%)[d]	ORAC[e]
		eeAChE[a]	eqBuChE[b]			
27	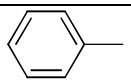	2.439 ± 0.08	4.660 ± 0.02	1.9	57.3 ± 0.34	0.55 ± 0.04
28	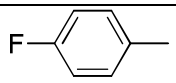	0.173 ±0.09	5.134 ±0.03	29.6	61.8 ± 0.42	1.03 ± 0.02
29	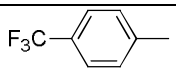	0.141±0.06	2.137 ±0.04	15.1	74.9 ± 0.72	0.72 ± 0.05
30	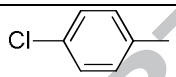	0.231 ± 0.04	1.109 ±0.07	4.8	60.8 ± 0.56	0.82 ± 0.03
31		0.251 ±0.02	0.392 ±0.06	1.5	62.4 ± 0.67	2.30 ± 0.14
32	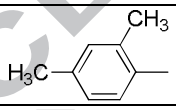	0.298 ±0.01	0.415 ±0.01	1.39	69.9 ± 0.42	2.39 ± 0.08
33	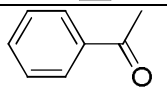	14.21 ±0.16	13.37 ±0.13	0.9	53.9 ± 0.66	2.45 ± 0.04
34	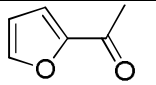	0.048 ± 0.002	2.605 ±0.05	54.2	82.2 ± 1.13 (9.2 ± 0.15)[f]	3.52 ± 0.23
35	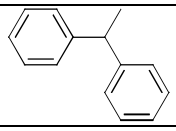	0.061±0.007	3.352 ±0.11	54.9	80.6 ± 1.08 (11.75 ± 0.10)[f]	1.89 ± 0.07

36	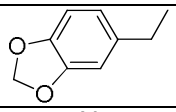	0.131±0.02	4.249 ±0.08	33.8	71.8 ± 0.78	3.46 ± 0.15
37	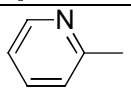	0.112 ±0.04	0.88 ± 0.002	7.8	70.9 ± 0.82	2.19 ± 0.12
38	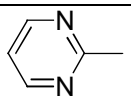	0.036 ±0.003	2.778 ±0.04	77.1	80.9 ± 0.94 (10.11 ± 0.06)[f]	2.84 ± 0.11
Donepezil	-	0.039 ± 0.002	3.36 ± 0.2	86.1	n.t	n.t
Curcumin	-	-	-	-	53.8 ± 0.63 (21.81 ± 0.16)[f]	n.t

[a] 50% inhibitory concentration (means ± SD of three experiments) of AChE from electric eel.
[b] 50% inhibitory concentration (means ± SD of three experiments) of BuChE from equine serum.
[c]SI selectivity index for AChE; IC_{50}eeBuChE/eqIC_{50} AChE.
[d] Inhibition of self-induced $A\beta_{1-42}$ aggregation (25μM) by tested inhibitors at 25μM by thioflavin-T based fluorescence method (means ± S.D of three experiments)
[e]Data are expressed as μmol of trolox equivalent/μmol of tested compound.
[f]IC_{50} value was determined from dose-response curves. Data are expressed as means ± S.D of three independent experiments; n.t. -not tested.

0.141μM) consist of the trifluoromethyl substituent at phenyl ring appeared as most potent among them. In contrast to this, compounds **31** (IC_{50} = 0.251μM) and **32** (IC_{50} = 0.298μM) containing electron-donating groups such as *p*-methyl and di-methyl, in the terminal phenyl ring showed quite better activity than those compounds which comprises of un-substituted phenyl ring (compound **27**, IC_{50} = 2.439μM). Hence, in this sub-series, the trend obtained in inhibitory potency against AChE is follow as: *p*-CF_3> *p*-F> *p*-Cl> *p*-Methyl> 2,4-dimethyl>H.

Furthermore, the replacement of phenyl group with other heterocyclic moieties leads to significant improvement in ChEls inhibitory potencies as well as selectivity of the compounds. For instance, compound **34** having furoyl group at terminal position and compound **35** with diphenyl ring exhibited 2.9 and 2.3 fold rise in inhibitory potency, respectively. Moreover, **34** and **35** showed better selectivity for AChE over BuChE, as compared to most active compound **29** of the phenyl substituted sub-series. The overall results of this study undoubtedly indicated that compound **38** comprising a terminal pyrimidine ring attached to piperazine linker, showed excellent AChE inhibitory activity among the entire series with an IC_{50} = 0.036μM and is

slightly higher than Donepezil (IC_{50} = 0.039µM). Moreover, its high selectivity index, i.e., 77.1 fold is indicative of its favorable binding affinity for AChE over the BuChE. Almost all the tested compounds exhibited a comparatively lower inhibitory potency against BuChE, with IC_{50} values ranging from 0.392 to 13.37µM indicating their preferable selectivity towards AChE. However, compounds **34** and **38** showed comparatively better selectivity for AChE than other tested derivatives. This selectivity profile may prove to be beneficial to diminish peripheral cholinergic side effects and would surely bestow lower toxicity.

2.3. Kinetic study of AChE inhibition

To gain further insight into the mechanism of action of compound **38,** Lineweaver-Burk double reciprocal plots for AChE inhibition were generated and are shown in Figure 3. The interception of the lines in the Lineweaver-Burk plot above the x-axis with both increased slope (decreased Vmax) and intercepts (higher Km) at increasing concentrations of the inhibitor, indicated a mixed-type inhibition, which verifies that compound **38** might be able to interact with both the catalytic active site (CAS) and peripheral anionic site (PAS) of AChE.

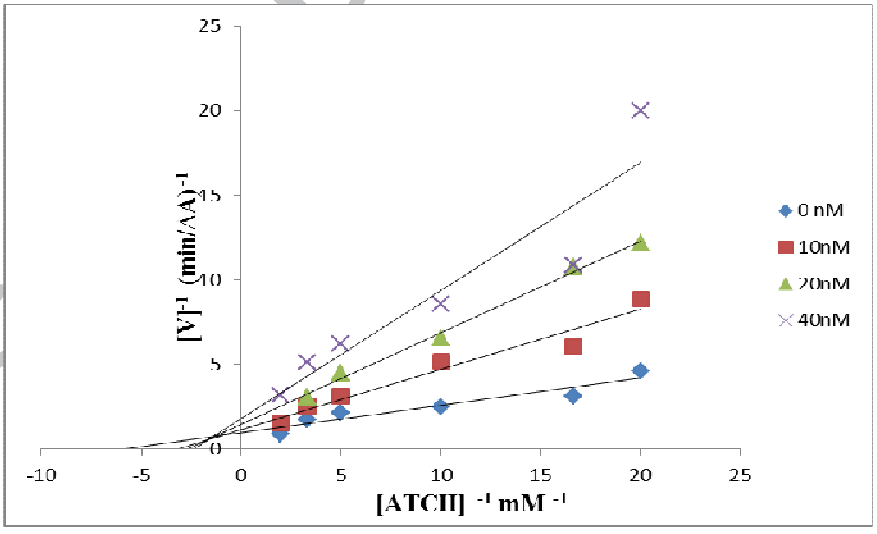

Fig 3. Lineweaver-Burk plot for the Inhibition of AChE by compound **38**

2.4. Inhibition of self mediated $A\beta_{1-42}$ aggregation

Targeting self-induced $A\beta_{1-42}$ aggregation represents an emerging approach for discovering drug candidates for AD. $A\beta_{1-42}$ has a high tendency to form fibrils and aggregates and its oligomers are neurotoxic that cause membrane disruption in neuronal cells.[20] To scrutinize the capability of target compounds (**27-38**) to inhibit the self-mediated $A\beta_{1-42}$ aggregation, the Thioflavin T (ThT) fluorescence assay [21] was implemented. Curcumin was taken as positive control because it is best known anti-amyloidogenic agent. Most of test compounds showed better inhibitory activity against $A\beta_{1-42}$ aggregation (1-1.5 folds) at 25μM when compared to the curcumin (Table 1). It was observed that the introduction of an electron rich substituent as in compounds **31** (62.4%) and **32** (69.9%) exhibited significant improvement towards inhibition of $A\beta_{1-42}$ aggregation. Furthermore, other derivatives (**34-38**), which consist of different heterocyclic rings at their terminal end offered a noticeable improvement in inhibition of $A\beta_{1-42}$ aggregation. The most profound inhibition was distinguished in compound **34**, **35** and **38** having furoyl, diphenyl and pyrimidine moieties, respectively inhibited more than 80% of $A\beta_{1-42}$ aggregation which was nearly 1.5 folds greater than inhibition by curcumin. All the three derivatives, achieved IC_{50} values much lower than that of curcumin (IC_{50}= 21.8 μM) as shown in Table 1. The combined result of β-amyloid and AChE inhibition studies suggests that these derivatives act as dual AChE inhibitors. This kind of inhibitors is often gifted with Aβ anti-aggregating properties, which arises either from the blockade of the AChE peripheral anionic site (PAS) or from a direct interaction with Aβ (blockade of spontaneous Aβ aggregation), and in the latter case it is likely due to the presence of curcumin fragment in the designed inhibitors.

2.5. Inhibition of $A\beta_{1-42}$ aggregation observed by Transmission Electron Microscopy (TEM)

Additionally, $A\beta_{1-42}$ aggregation potential of the most potent derivatives **34** and **38** was also evaluated by TEM study. After incubation at 37°C for 72 h, $A\beta_{1-42}$ alone aggregated into mature, denser and bulkier aggregates (Figure 4b), as compared to disaggregated $A\beta_{1-42}$ alone (Figure 4a) kept at 0°C. However, disaggregation effects were clearly visible upon treatment of compounds **34** and **38** for 72h (25μM each) and few Aβ fibrils were observed (Figure 4d, 4f), as compared to standard curcumin (Figure 4c).

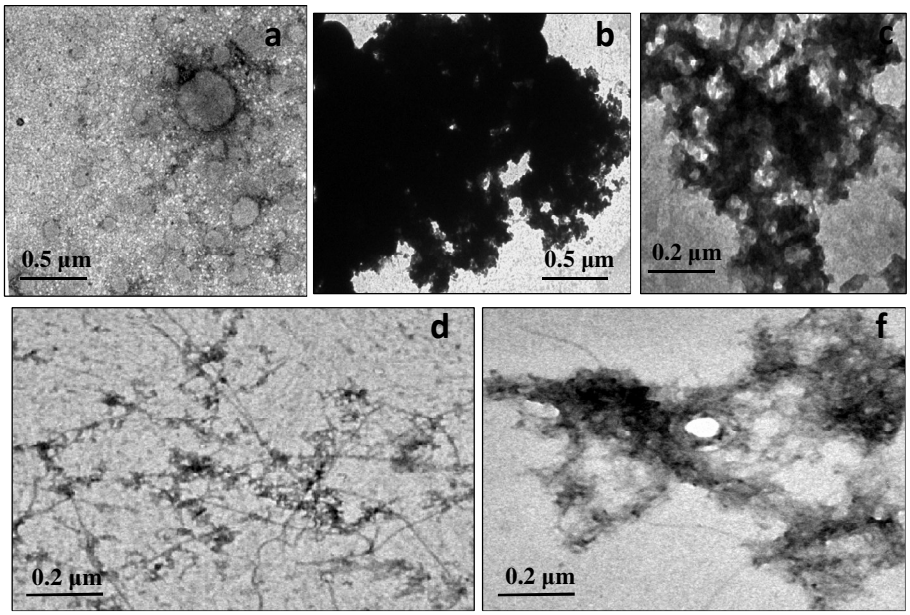

Fig 4. TEM images for Aβ-induced aggregation and test compound induced Aβ disaggregation: (a) 25µM $A\beta_{1-42}$ alone at 0 h (b) 25µM $A\beta_{1-42}$ alone at 24 h, 37℃ (c) 25µM $A\beta_{1-42}$ and 25µM curcumin (d) 25µM $A\beta_{1-42}$ and 25µM compound **34** (f) 25µM $A\beta_{1-42}$ and 25µM compound **38**

Thus, the results of TEM are consistent with ThT binding assay where compounds **34** and **38** potentially inhibit Aβ aggregation noticeably through direct interaction or by blocking PAS site of AChE.

2.6. Molecular docking study with AChE and BuChE

In order to study the binding mode and selectivity of most active compounds **34** and **38** with two cholinesterases, TcAChE (PDB code: 1EVE) and HuBuChE (PDB code: 4TPK), molecular docking was carried out using the docking program DS Client v 4.0 package. The active site of TcAChE enzyme consists of the catalytic anionic site (CAS) containing Trp84 and Phe330 residues and the peripheral anionic site (PAS) comprising mainly of Tyr70, Asp72, Tyr121, Tyr334, and Trp279 residues. Compound **38**, with strong inhibitory activity and high selectivity to AChE, exhibited multiple binding modes with AChE. The 1,3-indandione moiety adopted an appropriate orientation for its interaction with CAS near the bottom of the gorge, via the σ–π interaction with indole ring of Trp84 residue. The binding affinity can also be attributed to the π -π stacking interaction between the terminal pyrimidine ring and Trp279 residue of PAS site. Moreover, phenyl ring, present between

piperazine linker and indandione moiety, engage in π –π stacking interaction with Phe331 residue (Figure 5a, 5b).

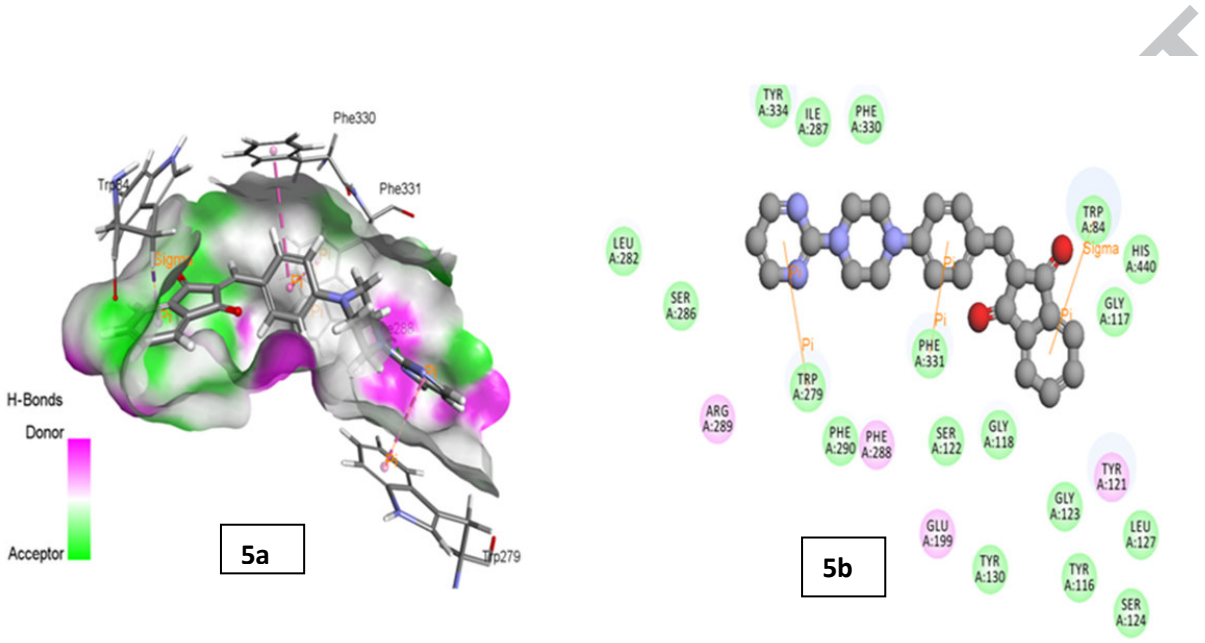

Fig 5. Docking simulation of compound **38** with TcAChE: (a) Stereoviews looking down the gorge of TcAChE binding with compound **38**. (b) 2D schematic diagram of docking model of compound **38** with TcAChE. Hydrogen-bond interactions as blue dashed line, π-π and cationic- π interactions are represented by an orange line with symbols indicating the interaction

In compound **34**–TcAChE complex, both phenyl ring and indole ring of 1,3-indandione moeity simultaneously stacked against the indole ring of Trp279 residue via π-π stacking. Furthermore, binding affinity was also contributed by furan ring present at terminal end establishes σ-π interaction with Trp84 residue of CAS (Figure 6a, 6b). The binding mode of compounds **34** and **38** with BuChE revealed that they also occupy the large catalytic cavity of BuChE and establishes π-π stacking interactions between aromatic Tyr332 residue and phenyl ring of the compound. However, there were no other significant interactions found in compound **34**–BuChE/ **38**–BuChE complex (Figure 7a, 7b). Meanwhile, the calculated binding free energy of compounds **34** and **38** with AChE is lower than that with BuChE.

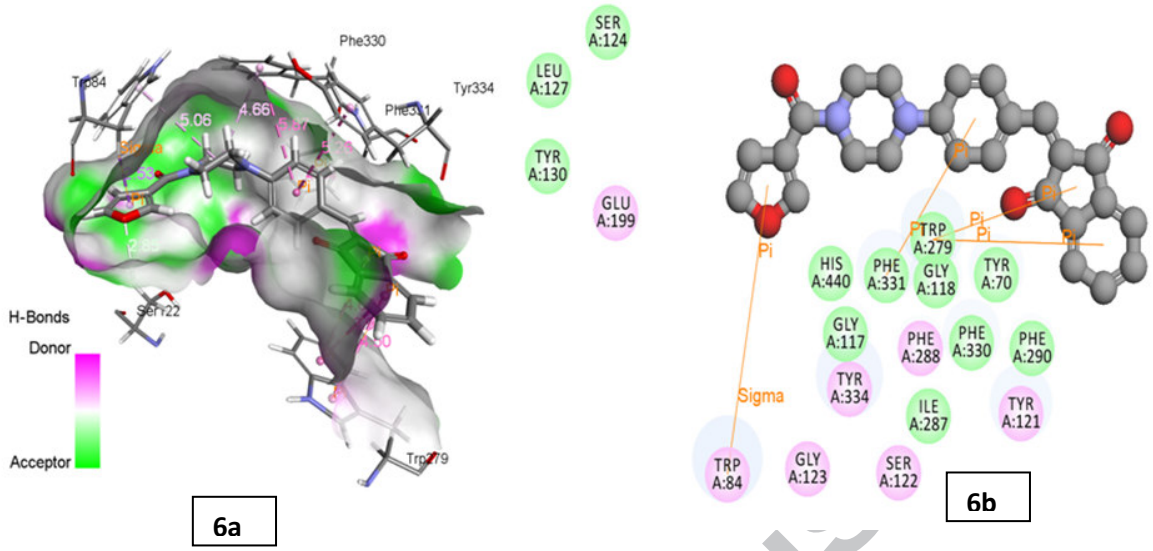

Fig 6. Molecular docking studies of compound **34** with TcAChE: (a) Stereoviews TcAChE binding with compound **34**, showing hydrogen bond donors and acceptors residues around compound**.** (b)2D schematic diagram of docking model of compound **34** with TcAChE. Residues involved in hydrogen-bonding, charge or polar interactions are represented by magenta-coloured circles. Van der Waals interactions are represented by green circles. The solvent accessible surface of an atom is represented by a blue halo around the atom. Hydrogen-bond interactions as blue dashed line, π-π and cationic- π interactions are represented by an orange line with symbols indicating the interaction

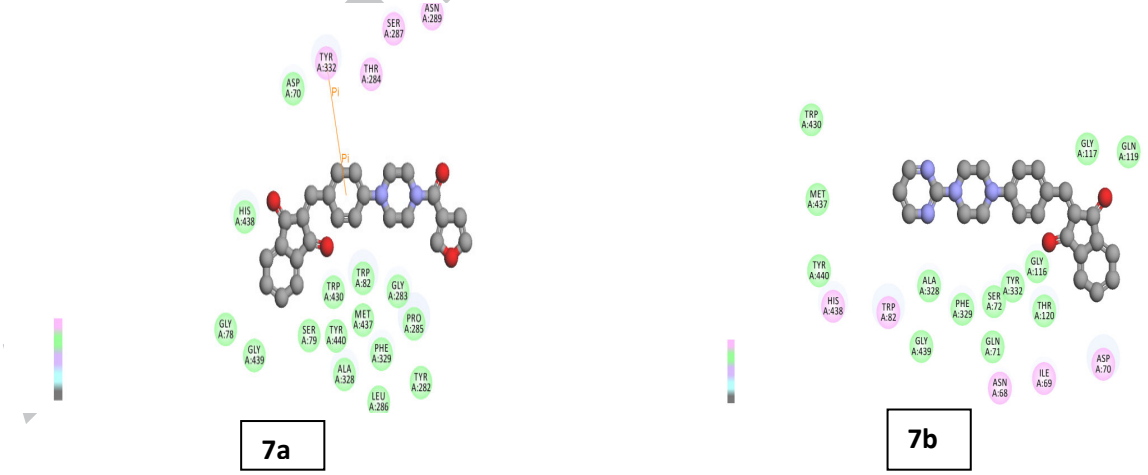

Fig 7 (a) 2D schematic diagram of docking model of compound **34** with HuBuChE. Residues involved in hydrogen-bonding, charge or polar interactions are represented by magenta-colored circles. Van der Waals interactions are represented by green circles. The solvent accessible surface of an atom is represented by a blue halo around the atom. Hydrogen-bond interactions as blue dashed line (b) 2D schematic diagram of docking model of compound **38** with HuBuChE. Residues involved in hydrogen-bonding, charge or polar interactions are represented by magenta-colored circles. Van der Waals interactions are represented by green circles. The solvent accessible surface of an atom is represented by a blue halo around the atom. Hydrogen-bond interactions as blue dashed line.

Thus, these compounds exhibited satisfactory selectivity for the inhibition of AChE over BuChE and exhibited a dual binding mode of action, i.e. they can simultaneously interact with CAS and PAS site of AChE enzyme.[22]

2.8 Antioxidant activity by ORAC-FL method

Oxidative stress plays a pivotal role in the progression of AD and antioxidant therapy may contribute significant role in the treatment of AD.[6] In this regard, antioxidant activities of synthesized compounds (**27-38)** were assessed by the well-established ORAC-FL method.[23] Results shown that these all compounds proved moderate to good antioxidant capacities ranging from 0.55 to 3.52 times the Trolox value (Table 1). As consistent with AChE and ThT results, compounds having furoyl (**34**), piperonyl (**36**) and pyrimidyl (**38**) ring in their molecular frame possessed admirable antioxidant activity in the entire series. The ORAC-FL values were recorded 3.52, 3.46 and 2.84 trolox equivalents for compounds **34**, **36** and **38**, respectively. The antioxidant potential of compounds **34**, **36** and **38**, advocated their multifunctional endeavors to defend against AD.

2.9. Intracellular antioxidant activity

The intracellular antioxidant activity of compounds **34** and **38** (5, 10 and 20μM) against H_2O_2-induced ROS in SH-SY5Y cells were assessed by DCFH-DA fluorescent assay. Exposure of SH-SY5Y cells to H_2O_2 (200μM) increased the intracellular ROS accumulation by about 1.58 fold, $p < 0.001$, in 24h. Treatment with compound **34,** fashioned a dose dependent inhibitory effect (5μM, $p < 0.05$; 10μM, $p < 0.01$ and 20μM, $p < 0.001$) on ROS formation without affecting basal levels of ROS. On the other hand, compound **38** also exerted a considerable inhibitory effect at the dose of 10μM and 20μM (Figure 8a). These results visibly suggested that compounds **34** and **38** have immense potential

to overcome oxidative load in SH-SY5Y cells, which make them capable to save cell against oxidative damage.

2.10. Neuroprotection activity against H_2O_2 induced neurotoxicity

AD is a deadly progressive neurodegenerative disorder and ongoing neuron degeneration is the result of excessive ROS production as well Aβ accumulation.[24] Therefore, neuroprotective strategy considered as permanent therapy for AD besides other symptomatic relief strategy. To achieve this approach, the neuroprotective potential of the compounds **34** and **38** against H_2O_2-induced neurotoxicity in SH-SY5Y cells were assessed by cell viability assay at three different concentrations (5, 10 and 20 µM). Treatment of cells with H_2O_2 (200µM) for 24 h, resulted in a marked decrease in cell viability (46%, $p < 0.001$) as compared to untreated control. The co-treatment of cells with compounds **34** and **38** ameliorated H_2O_2-induced neurotoxicity in a concentration dependent manner (Figure 8b). Compound **34** exhibited the highest protective capability at 10µM ($p < 0.01$) while compound **38** showed similar protective ability at 20µM ($p < 0.01$). To validate these results, phase contrast microscopy was employed to visualize the neuroprotective effect of the compound against H_2O_2 induced neurotoxicity (Figure 8c).

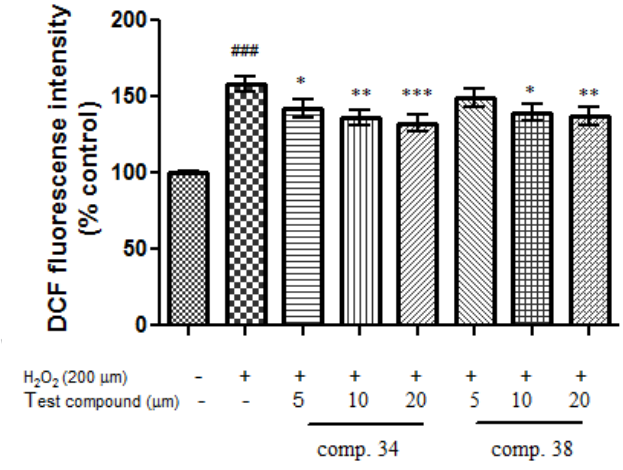

8a

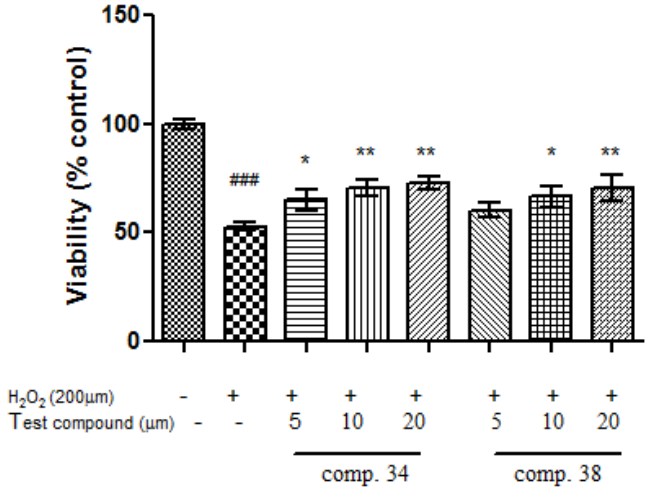

8b

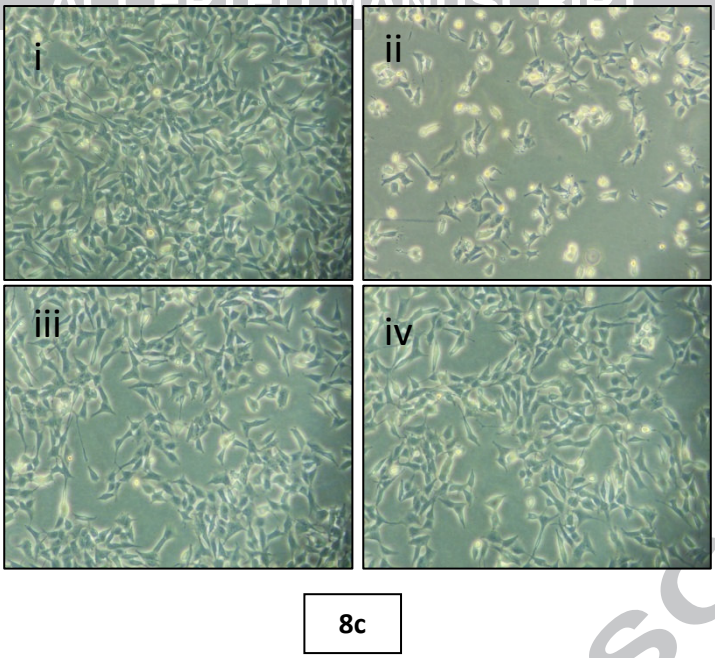

Fig.8. Compounds **34** and **38** significantly reduced oxidative stress and exhibited the neuroprotective effect on SH-SY5Y cells: (a) effect of compounds **34** and **38** on diminution of oxidative stress in DCF florescence assay. (b) Phase-contrast micrographs showing H_2O_2-induced neurotoxicity and neuroprotection of compound **34** and compound **38** in SH-SY5Y cells. (i) Cells without treatment (ii) H_2O_2 alone (200μM) (iii) Compound **34** (20μM) was given for 24 h with H_2O_2 (200μM) at 37° C. (iv) Compound **38** (20μM) was given for 24 h with H_2O_2 (200μM) at 37°C. All data were expressed as mean ±S.D of three experiments and each included triplicate sets. $^{\#}p < 0.05$, $^{\#\#}p < 0.01$, $^{\#\#\#}p < 0.001$ vs control; $^{*}p < 0.05$, $^{**}p < 0.01$, $^{***}p < 0.001$ vs H_2O_2 alone. Statistical analysis was performed using one way ANOVA followed by Bonferroni test.

Microscopic observations showed that a large number of H_2O_2-treated cells became rounded, vacuolated and floated, which clearly indicated apoptosis or necrosis in SH-SY5Y cells. However, the treatment with compounds **34** and **38** (20μM) shielded these morphological changes and significantly prevented the cell death induced by H_2O_2 toxicity in these cells. These results educe that compounds **34** and **38** successfully reduced H_2O_2 induced neurotoxicity in SH-SY5Y cells.

2.11. Neuroprotective activity against Aβ induced neurotoxicity

To elucidate extensive neuroprotective potential of compounds **34** and **38**, they were also tested against $A\beta_{1-42}$ induced neurotoxicity in SH-SY5Y neuroblastoma cells. Results showed that co-treatment of cells with both compounds for 24h ameliorated Aβ induced neurotoxicity in a concentration dependent manner and exhibited neuroprotective effects at concentration ranging from 5 to 20μM (Figure 9a). The similar neuroprotective ability of compounds **34** and **38** were also

visualized by microscopic imaging where both compounds restored apoptosis associated morphological changes in SH-SY5Y cells (Figure 9b).

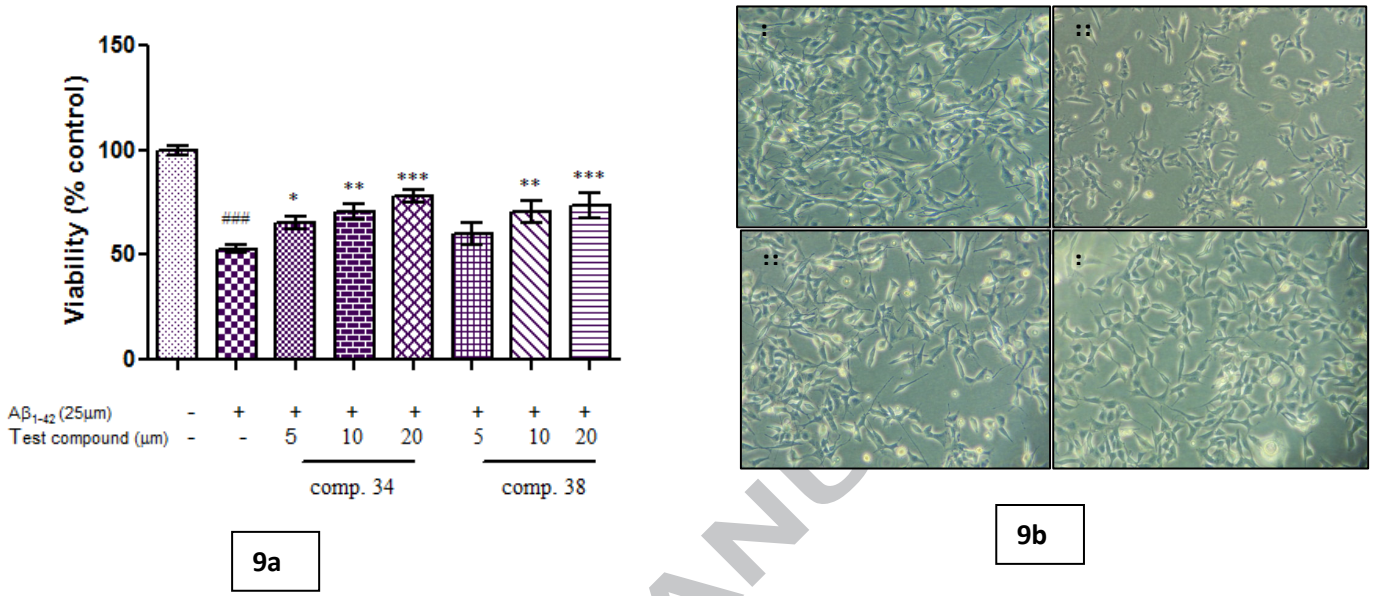

Fig 9. Neuroprotection against Aβ-induced toxicity: (a) Compounds **34** and **38** were tested for neuroprotective activity against Aβ toxicity in SH-SY5Y cell. Results are expressed as percent viability compared to untreated control. All data were expressed as mean ±S.D of three experiments and each included triplicate sets. $^{\#}p < 0.05$, $^{\#\#}p < 0.01$, $^{\#\#\#}p < 0.001$ vs control; $^{*}p < 0.05$, $^{**}p < 0.01$, $^{***}p < 0.001$ vs $A\beta_{1-42}$ alone. Statistical analysis was performed using one way ANOVA followed by Bonferroni test. (b) Phase-contrast micrographs showing Aβ-induced neurotoxicity and neuroprotection of **34** and **38** in SH-SY5Y cells. (i) Cells without treatment. (ii) Aβ alone (25μM). (iii) Compound **34** (20μM) was given for 24 h with Aβ (25μM) at 37° C. (iv) Compound **38** (20μM) was given for 24 h with Aβ (25μM) at 37° C

These results suggested that these novel compounds exerted marked neuroprotection against Aβ-induced neurotoxicity. The neuroprotective nature of these compounds confirms their potential as multifunctional agent which not just able to maintain choline levels, but they likewise possess the capacity to block progression of nerve cell degeneration.

2.12. Cytotoxicity study on normal neuronal cells

Additionally, toxicity of compounds **34** and **38** were assessed in SH-SY5Y neuronal cell line with different concentrations ranging from 1-100 μM. After exposing the cells to these compounds for 48 h, the cell viability was evaluated by 3-(4, 5-dimethylthiazol-2-yl) -2, 5-diphenyltetrazolium (MTT)

assay. The results showed a dose-dependent effect of the tested compounds **34** (1µM: 98.1 ± 3.6%; 5µM: 96.4 ± 3.2%; 10µM: 95.3 ± 4.6%; 25µM: 93.9 ± 2.7%; 50µM: 89.6 ± 3.1%; 75µM: 86.3 ± 2.6% and 100µM: 82.3 ± 3.5%) and **38** (1µM: 98.1 ± 3.6%; 5µM: 96.4 ± 3.2%; 10µM: 95.3 ± 4.6%; 25µM: 93.9 ± 2.7%; 50µM: 89.6 ± 3.1%; 75µM: 86.3 ± 2.6% and 100µM: 82.3 ± 3.5%) on the viability of SH-SY5Y cells at different concentrations in the range from 1µM to 100µM. Interestingly, both compounds did not produce a significant cytotoxic effect on the cells up to 100 µM concentration after 24 h treatment (Figure 10).

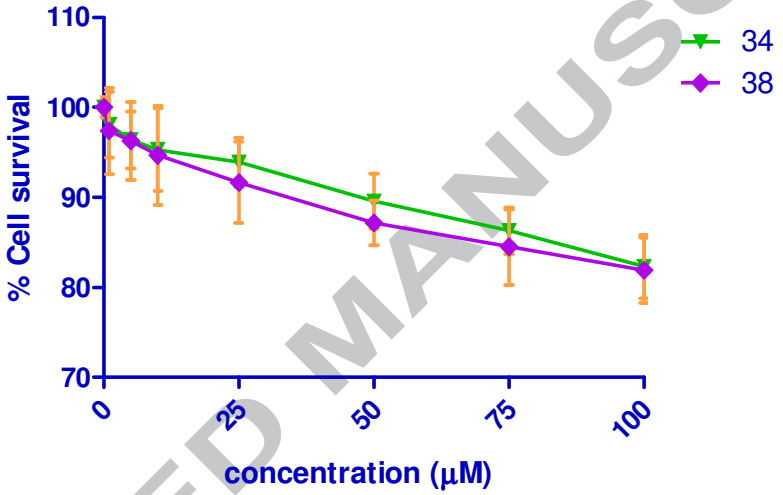

Fig 10. Effect of compounds **34** and **38** on the viability of SH-SY5Y cells. The cells were incubated with the indicated concentrations of the tested compounds for 48 h. The cell viability was assessed by MTT assay. Percentages of the cell viability are presented as mean ± SEM from 3 independent experiments

Thus, the results indicate that these new compounds did not exhibit cytotoxicity.

2.13. In-silico physicochemical and pharmacokinetic study

Primarily pharmacokinetic properties of most active compounds **34** and **38** were evaluated by Molinspiration and Biovia discovery studio software (Table 2, Figure 11).

Table 2 Physicochemical and Pharmacokinetic properties of most active compound **34** and **38**

Comp. No	Mol. Wt.	AlogP98	HBA[b]	HBD[a]	NRB[a]	Volume	PSA[a]	BBB Level	Absorption Level	Hepatotoxicity Level
34	412	3.67	6	0	3	363	71.16	2	0	0
38	396	3.77	6	0	3	355	63.82	1	0	0

a HBA: H-bond acceptor, HBA: H-bond donor, NRB: number of rotatable bonds

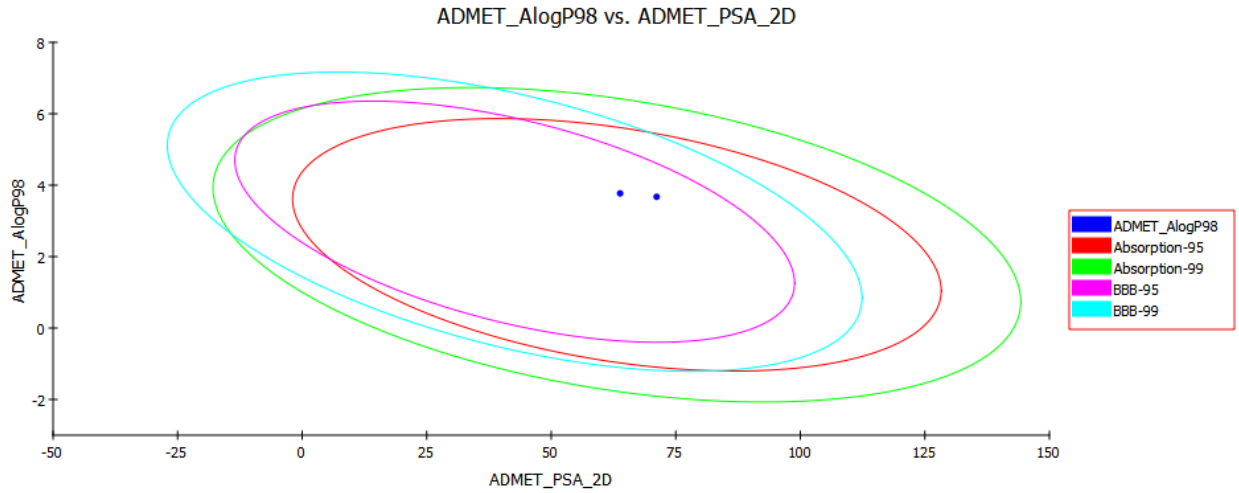

Fig 11. Discovery Studio 2.1 (Accelrys, San Diego, CA) ADMET Descriptors, 2D polar surface area (PSA 2D) in A^{02} for compounds **34** and **38** are plotted against their corresponding calculated partition coefficient (ALogP98). The area cover by the ellipses is a prediction of good intestinal absorption absorption and BBB with no violation of ADMET properties.

,Results showed that both compounds obey Lipinski rule[25] of 5 [molecular weight (Mol. Wt.) ≤ 500, HBD ≤ 5, HBA ≤ 10, log P ≤ 5.0 and <10 number of rotatable bonds]. The polar surface area (PSA) is an important descriptor to predict oral bioavailability and blood brain barrier (BBB) penetration ability of any new molecule. Here, both compounds positively showed acceptable PSA, which indicates their good oral bioavailability and BBB penetration when administered *in-vivo*. Moreover, due to presence of appropriate number of rotatable bonds compounds **34** and **38** are likely to provide optimal flexibility at the targeted site in the brain to exert desired biological activity. It was also examined that compounds **34** and **38** displayed an absorption level '0' which support their excellent human intestinal absorption (HIA) property.[26] Hepatotoxicity always remains a major concern for any

new drug development program and compounds **34** and **38** were found non-hepatotoxic. This study evidently indicates the suitability of compounds **34** and **38** as drug like candidates for future.

3. Conclusion

In conclusion, herein we have successfully designed and synthesized a novel series of 2-(4-(4-substituted piperazin-1-yl)benzylidene)-1H-indene-1,3(2H)-diones derivatives as potent multitarget agents for the treatment of AD. Synthesized derivatives **27-38** pointedly inhibited AChE and Aβ aggregation. Compounds **34** and **38** were found most active inhibitor among entire series and inhibited AChE selectively over BuChE and also excellently inhibited Aβ aggregation as compared to standard drug Donepezil. In-silico docking studies of compounds **34** and **38** further confirmed their preferable binding with AChE over BuChE and also displayed interaction with key amino acids of Aβ. Moreover, **34** and **38** acted as potent antioxidant agents in ORAC-FL assay and significantly abridged H_2O_2 induced oxidative stress concentration dependently in DCF-fluorescence assay in SH-SY5Y cells. Furthermore, compounds **34** and **38** exhibited potential neuroprotective effects in H_2O_2 and Aβ induced neurodegeneration in SH-SY5Y cells. In addition to this, both derivatives did not exert toxicity against normal neuronal SH-SY5Y cells up to 100μM concentration and displayed favorable drug like properties in primarily pharmacokinetic studies. Thus, novel indandione derivatives **34** and **38** emerged as potent and safe multifunctional agents against AD and may develop as suitable multifunctional agents for the management of AD in the future.

4. Experimental section

4.1. Chemistry

All the chemicals and reagents were obtained from Sigma Aldrich (St. Louis, MO, USA), Alfa Aesar (Massachusetts), S.D Fine Chemicals (India) and Merck (Darmstadt, Germany) and solvents for reaction medium were dried by standard methods. Melting points were taken in open capillaries using model KSPII, KRUSS, (Germany). The nuclear magnetic resonance (NMR) spectra were recorded on high resolution Jeol-400MHz NMR spectrophotometer (USA). Mass

spectra were recorded on an Agilent 6310 Ion trap LC/MS and elemental analysis (C, H and N) was carried on Elementaranalysensysteme.

4.2. General procedure for synthesis of 4-(4-substituted piperazin-1-yl) benzaldehyde (14-25)

A mixture of substituted piperazine (10 mmole), 4-fluorobenzaldehyde (10 mmole) and K_2CO_3 (2 mmole) were refluxed at 130^0C in DMF for 15-24h. Thereafter, the reaction mixture was poured into ice cold water and the precipitate that appeared was filtered and dried to accomplish formyl derivatives (**14-25)** in a yield of 80-90%.

4.2.1. 4-(4-phenylpiperazin-1-yl) benzaldehyde (14)

White solid; yield 85% ; mp: 125-127^{0}C ;^{1}H NMR ($CDCl_3$,400 MHz): δ3.35 (t, 4H, piperazine, J= 4.9Hz), 3.57 (t, 4H, piperazine, J= 5.3 Hz), 6.91-6.98 (m, 5H, Ar-H), 7.28-7.32 (m, 2H, Ar-H, J= 8.4 Hz), 7.78 (d, 2H, Ar-H, J= 8.4 Hz), 9.80 (s, 1H, CH); LC–MS: m/e 267 (M+1).

4.2.2. 4-(4-(4-fluorophenyl)piperazin-1-yl)benzaldehyde (15)

White solid; yield 80% ; mp: 130-132^{0}C ; ^{1}H NMR($CDCl_3$,400 MHz): δ3.25 (t, 4H, piperazine, J= 4.9 Hz), 3.55 (t, 4H, piperazine, J= 4.9 Hz), 6.90-7.02 (m, 6H, Ar-H), 7.78 (d, 2H, Ar-H, J= 9.1 Hz), 9.80 (s, 1H, CH); LC–MS: m/e 285 (M+1).

4.2.3.4 -(4-(trifluoromethyl) piperazin-1-yl) benzaldehyde (16)

White solid; yield 87% ; mp: 185-187^{0}C ; ^{1}H NMR($CDCl_3$,400 MHz): δ3.47 (t, 4H, piperazine, J= 4.9 Hz), 3.60 (t, 4H, piperazine, J= 4.9 Hz), 6.96 (dd, 4H, Ar-H, J= 8.7 Hz), 7.52 (d, 2H, Ar-H, J= 9.1 Hz), 7.80 (d, 2H, Ar-H, J= 9.1 Hz), 9.81 (s, 1H, CH); LC–MS: m/e 335(M+1).

4.2.4. 4-(4-(4-chlorophenyl) piperazin-1-yl) benzaldehyde (17)

White solid; yield 85% ; mp: 147-149^{0}C ; ^{1}H NMR($CDCl_3$,400 MHz): δ3.31 (t, 4H, piperazine, J= 4.6 Hz), 3.56 (t, 4H, piperazine, J= 4.9 Hz), 6.86 (d, 2H, Ar-H, J= 9.1 Hz), 6.96 (d, 2H, Ar-H, J= 8.4 Hz), 7.22 (d, 2H, Ar-H, J= 8.0 Hz), 7.79 (d, 2H, Ar-H, J= 9.1 Hz), 9.80 (s, 1H, CH); LC–MS: m/e 301 (M+1).

4.2.5. 4-(4-(p-tolyl)piperazin-1-yl)benzaldehyde (18)

White solid; yield 88% ; mp: 145-147^{0}C ; ^{1}H NMR($CDCl_3$,400 MHz): δ2.29 (s, 3H, CH_3), 3.28 (t, 4H, piperazine, J= 4.9 Hz), 3.55 (t, 4H, piperazine, J= 5.3 Hz), 6.89 (d, 2H, Ar-H, J= 8.3 Hz), 6.97 (d, 2H, Ar-H, J= 9.1 Hz), 7.11 (d, 2H, Ar-H, J= 8.4 Hz), 7.78 (d, 2H, Ar-H, J= 9.1 Hz), 9.79 (s, 1H, CH); LC–MS: m/e 281(M+1).

4.2.6. 4-(4-(2,4-dimethylphenyl)piperazin-1-yl)benzaldehyde (19)

White solid; yield 78% ; mp: 155-157^{0}C ; ^{1}H NMR($CDCl_3$,400 MHz): δ2.28 (s, 3H, CH_3), 2.31 (s, 3H, CH_3), 3.02 (t, 4H, piperazine, J= 4.9 Hz), 3.55 (t, 4H, piperazine, J= 4.9 Hz), 6.93-7.03 (m, 5H, Ar-H), 7.77 (d, 2H, Ar-H, J= 9.1 Hz), 9.79 (s, 1H, CH); LC–MS: m/e 295(M+1)

4.2.7. 4-(4-benzoylpiperazin-1-yl)benzaldehyde (20)

White solid; yield 78%; mp:101-103^{0}C; ^{1}H NMR($CDCl_3$,400 MHz):δ3.30-3.84 (m, 8H, piperazine), 6.85 (d, 2H, Ar-H, J= 9.1 Hz), 7.32-7.37 (m, 5H, Ar-H), 7.70 (d, 2H, Ar-H, J=9.1 Hz), 9.72 (s, 1H, CH), LC–MS: m/e 295 (M+1).

4.2.8. 4-(4-(furan-3-carbonyl)piperazin-1-yl)benzaldehyde (21)

White solid; yield 86% ; mp: 98-100^{0}C ; ^{1}H NMR($CDCl_3$,400 MHz):δ3.51 (t, 4H, piperazine, J= 5.3Hz), 4.01 (s, 4H, piperazine), 6.52 (dd, 1H, Ar-H, J= 3.4 Hz), 6.95 (d, 2H, Ar-H, J= 9.1 Hz), 7.08 (d, 1H, Ar-H, J= 3.8 Hz), 7.52 (s, 1H, Ar-H), 7.77 (d, 2H, Ar-H, J= 9.1 Hz), 9.81 (s. 1H, CH); LC–MS: m/e 285(M+1).

4.2.9. 4-(4-benzhydrylpiperazin-1-yl)benzaldehyde (22)

White solid; yield 82% ; mp: 122-124^{0}C ; ^{1}H NMR($CDCl_3$,400 MHz): δ2.54 (t, 4H, piperazine, J= 4.9Hz), 3.39 (t, 4H, piperazine, J= 4.9 Hz), 4.26 (s, 1H, CH), 6.87 (d, 2H, Ar-H, J= 8.4 Hz), 7.18-7.31 (m, 6H, Ar-H), 7.44 (d, 4H, Ar-H, J= 7.6 Hz), 7.71 (d, 2H, Ar-H, J= 9.1 Hz), 9.76 (s, 1H, CH); LC–MS: m/e 357(M+1).

4.2.10. 4-(4-(benzo[d][1,3]dioxol-5-ylmethyl)piperazin-1-yl)benzaldehyde (23)

White solid; yield 78%; mp:115-117^{0}C; ^{1}H NMR($CDCl_3$,400 MHz): δ2.57 (t, 4H, piperazine, J= 4.9Hz), 3.40 (t, 4H, piperazine, J= 4.9 Hz), 3.47 (s, 2H, CH_2), 5.95 (s, 2H, CH_2), 6.76 (s, 2H, Ar-H), 6.88-6.91 (m, 3H, Ar-H), 7.74 (d, 2H, Ar-H, J= 8.4 Hz), 9.77 (s, 1H, CH); LC–MS: m/e 325 (M+1).

4.2.11.4-(4-(pyridin-2-yl)piperazin-1-yl)benzaldehyde (24)

White solid; yield 82%; mp: 140-142^{0}C ; ^{1}H NMR($CDCl_3$,400 MHz): δ2.39 (s, 4H, piperazine), 3.36 (s, 4H, piperazine), 6.83 (d, 2H, Ar-H, J= 9.9 Hz), 7.24 (s, 2H, Ar-H), 7.75 (q, 4H, Ar-H, J= 9.1 Hz), 10.0 (s, 1H, CH); LC–MS: m/e 268(M+1).

4.2.12.4-(4-(pyrimidin-2-yl)piperazin-1-yl)benzaldehyde (25)

White solid; yield 79% ; mp: 138-140^{0}C ; ^{1}H NMR($CDCl_3$,400 MHz): δ3.51 (t, 4H, piperazine, J= 5.3 Hz), 4.00 (t, 4H, piperazine, J= 5.3 Hz), 6.55 (t, 1H, Ar-H, J= 4.4 Hz), 6.95 (d, 2H, Ar-H, J= 9.1 Hz), 7.78 (d, 2H, Ar-H, J= 8.4 Hz), 8.33 (d, 2H, J= 4.5 Hz), 9.79 (s, 1H, CH); LC–MS: m/e 269 (M+1).

4.3. General procedure for synthesis of 2-(4-(4-substituted piperazin-1-yl)benzylidene)-1H-indene-1,3(2H)-dione (27-38)

Piperidine (2mL) was added to a solution of formyl derivatives 14-25 (4 mmole) and 1,3-indandione (4 mmol) in 20mL of anhydrous ethanol. The reaction mixture was stirred for 3-6h and the precipitate that appeared was filtered and dried. The acquired crude products were purified by column chromatography using chloroform:methanol (98:02) as eluent.

4.3.1.2-(4-(4-phenylpiperazin-1-yl) benzylidene)-1H-indene-1,3(2H)-dione(27)

Yellow solid; yield 85%; mp: 210-212^{0}C; ^{1}HNMR ($CDCl_3$, 400 MHz): δ3.37(t, 4H, 2xCH_2, J= 6.0 Hz), 3.66(t, 4H, 2xCH_2, J= 5.7 Hz), 6.90-6.98 (m, 5H, Ar), 7.31(t, 2H, Ar, J= 7.8Hz), 7.74-7.76(m, 2H, Ar), 7.80(s, 1H, CH), 7.92-7.97(m, 2H, Ar), 8.55(d, 2H, Ar, J= 9.1 Hz); ^{13}C NMR ($CDCl_3$, 100 MHz): δ 46.6, 48.8, 113.2, 116.2, 120.3, 122.6, 123.5, 124.2, 129.2, 134.3, 134.6, 137.6, 139.8, 142.3, 146.9, 150.8, 153.9, 189.9, 191.3; LC-MS: m/z, 395 (M+1); Anal. Calcd for $C_{26}H_{22}N_2O_2$: C, 79.16; H, 5.62; N, 7.10Found: C, 79.47; H, 5.41; N, 7.35.

4.3.2. 2-(4-(4-(4-fluorophenyl) piperazin-1-yl)benzylidene)-1H-indene-1,3(2H)-dione (28)

Yellow solid; yield 76%; mp: 210-212^{0}C; ^{1}HNMR ($CDCl_3$, 400 MHz): δ 3.20(t, 4H, 2xCH_2, J= 5.3 Hz), 3.58 (t, 4H, 2XCH_2, J= 5.3 Hz), 6.84-6.96 (m, 6H, Ar), 7.67-7.69(m, 2H, Ar), 7.73(s, 1H, CH), 7.86-7.90(m, 2H, Ar), 8.87(d, 2H, Ar, J= 8.4Hz);LC-MS: m/z, 413 (M+1); Anal. Calcd for $C_{26}H_{21}FN_2O_2$: C, 75.71; H, 5.13; F, 4.61; N, 6.79Found: C, 75.46; H, 5.34; N, 7.09.

4.3.3.2-(4-(4-(4-(trifluoromethyl)phenyl)piperazin-1-yl)benzylidene)-1H-indene-1,3(2H)-dione (29)

Yellow solid; yield 74%; mp: 240-242^{0}C; ^{1}HNMR ($CDCl_3$, 400 MHz): δ 3.49(t, 4H, 2X CH_2, J= 4.9), 3.68(t, 4H, 2XCH_2, J= 5.3 Hz), 6.93-6.97(m, 4H, Ar), 7.52(d, 2H, Ar, J= 8.4 Hz), 7.74-7.76(m, 2H, Ar), 7.80(s, 1H, CH), 7.93-7.97(m, 2H, Ar), 8.55(d, 2H, Ar, J= 9.1Hz);LC-MS: m/z, 463 (M+1);Anal. Calcd for $C_{27}H_{21}F_3N_2O_2$: C, 70.12; H, 4.58; N, 6.06Found:C, 69.80; H, 4.87; N, 6.47

4.3.4. 2-(4-(4-(4-chlorophenyl)piperazin-1-yl)benzylidene)-1H-indene-1,3(2H)-dione (30)

Yellow solid; yield 65%; mp: 222-225^{0}C; ^{1}HNMR ($CDCl_3$, 400 MHz): δ 3.32(t, 4H, 2XCH_2, J= 5.7 Hz), 3.65(t, 4H, 2XCH_2, J= 5.3 Hz), 6.87(d, 2H, Ar, J= 9.1 Hz), 6.96(d, 2H, Ar, J= 9.1 Hz), 7.22-7.23(m, 2H, Ar), 7.72-7.77(m, 2H, Ar), 7.80(s, 1H, CH), 7.93-7.97(m, 2H, Ar), 8.54(d, 2H, Ar, J= 9.1 Hz);); LC-MS: m/z, 429 (M+1);Anal. Calcd for $C_{26}H_{21}ClN_2O_2$: C, 72.81; H, 4.94; N, 6.53 Found:73.19; H, 5.23; N, 6.21.

4.3.5. 2-(4-(4-(p-tolyl) piperazin-1-yl)benzylidene)-1H-indene-1,3(2H)-dione (31)

Yellow solid; yield 68%; mp: 198-200^{0}C; ^{1}HNMR ($CDCl_3$, 400 MHz): δ 2.29(s, 3H, CH_3), 3.29(t, 4H, 2XCH_2, J= 4.9 Hz), 3.64(t, 4H, 2X CH_2, J= 4.9 Hz), 6.88(d, 2H, Ar, J= 7.6 Hz), 6.96(d, 2H, Ar, J= 8.4 Hz), 7.11(d, 2H, Ar, J= 7.6 Hz), 7.34-7.75(m, 2H, Ar), 7.79(s, 1H, CH), 7.92-7.95(m, 2H, Ar), 8.53(d, 2H, Ar, J= 8.4 Hz); ^{13}C NMR ($CDCl_3$, 100 MHz): δ 20.4, 46.6, 113.1, 116.6, 122.6, 123.5, 124.2, 129.7, 129.9, 134.3, 134.5, 137.6, 139.8, 142.2, 146.9, 148.6, 148.9, 153.9, 187.7, 191.3; LC-MS: m/z, 409 (M+1);Anal. Calcd for $C_{27}H_{24}N_2O_2$: C, 79.39; H, 5.92; N, 6.86Found: C, 79.69; H, 5.79; N, 6.57

4.3.6. 2-(4-(4-(2,4-dimethylphenyl)piperazin-1-yl)benzylidene)-1H-indene-1,3(2H)-dione (32)

Yellow solid; yield 90%; mp: 170-172^{0}C; ^{1}HNMR ($CDCl_3$, 400 MHz): δ 2.29(s, 3H, CH_3), 2.32(s, 3H, CH_3), 3.03(t, 4H, 2XCH_2, J= 4.9 Hz), 3.62(t, 4H, 2XCH_2, J= 4.8Hz), 6.92-7.04(m, 5H, Ar), 7.73-7.76(m, 2H, Ar), 7.77(s, 1H, CH), 7.92-7.96(m, 2H, Ar), 8.34(d, 2H, Ar, J= 9.0 Hz);^{13}C NMR ($CDCl_3$, 100 MHz): δ 17.7, 20.7, 47.3, 51.6, 113.0, 113.2, 119.0, 122.6, 123.4, 124.1, 127.1, 131.7, 132.0, 132.5, 133.2, 134.3, 134.5, 137.5, 137.7, 139.8, 142.2, 146.9, 148.3,

154.2, 189.8, 191.4; LC-MS: m/z, 423 (M+1);Anal. Calcd for $C_{28}H_{26}N_2O_2$: C, 79.59; H, 6.20; N, 6.63Found: C,79.90; H, 6.01; N, 6.31

4.3.7.2-(4-(4-benzoylpiperazin-1-yl)benzylidene)-1H-indene-1,3(2H)-dione (33)

Yellow solid; yield 88%; mp: 260-262^{0}C; ^{1}HNMR ($CDCl_3$, 400 MHz): δ 3.48-3.95(m, 8H, 4XCH_2), 6.92(d, 2H, Ar, J= 8.4 Hz), 7.45(s, 5H, Ar), 7.74-7.76(m, 2H, Ar), 7.79(s, 1H, CH), 7.93-7.95(m, 2H, Ar), 8.52(d, 2H, Ar, J= 8.4 Hz);^{13}C NMR ($CDCl_3$, 100 MHz): δ 46.9, 113.4, 113.6, 122.7, 124.1, 124.9, 127.0, 127.2, 128.6, 130.1, 134.5, 134.7, 135.1, 137.3, 137.5, 139.8, 142.2, 146.7, 153.6, 189.7, 191.3;LC-MS: m/z, 423 (M+1);Anal. Calcd for $C_{27}H_{22}N_2O_3$: C, 76.76; H, 5.25; N, 6.63Found: C, 77.01, H, 5.45; N, 6.36.

4.3.8. 2-(4-(4-(furan-2-carbonyl) piperazin-1-yl)benzylidene)-1H-indene-1,3(2H)-dione (34)

Yellow solid; yield 78%; mp: 250-252^{0}C; ^{1}HNMR ($CDCl_3$, 400 MHz): δ 3.53(t, 4H, 2 X CH_2), 3.95(s, 4H, 2 XCH_2), 6.45-6.46(m, 1H, Ar), 6.86(d, 2H, Ar, J= 9.1Hz), 7.03(d, 1H, Ar, J= 3.0Hz), 7.45(s, 1H, Ar), 7.67-7.70(m, 2H, Ar), 7.73(s, 1H, CH), 7.87-7.90(m, 2H, Ar), 8.47(d, 2H, Ar, J= 9.1 Hz); ^{13}C NMR ($CDCl_3$, 100 MHz): δ 29.5, 46.5, 111.5, 113.2, 117.2, 122.7, 123.7, 124.6, 134.5, 134.7, 137.5, 139.8, 142.1, 144.0, 146.8, 147.6, 153.5, 159.1, 189.8, 191.3; LC-MS: m/z, 413 (M+1);Anal. Calcd for $C_{25}H_{20}N_2O_4$: C, 72.80; H, 4.89; N, 6.79 Found: C, 72. 49; H, 5.11; N, 6.44.

4.3.9. 2-(4-(4-benzhydrylpiperazin-1-yl)benzylidene)-1H-indene-1,3(2H)-dione (35)

Yellow solid; yield 85%; mp: 228-230^{0}C; ^{1}HNMR ($CDCl_3$, 400 MHz): δ 2.55(t, 4H, 2 X CH_2, J= 4.9 Hz), 3.48(t, 4H, 2 X CH_2, J= 4.9 Hz), 4.26(s, 1H, CH), 6.87(d, 2H, Ar, J= 8.4 Hz), 7.19-7.22(m, 2H, Ar), 7.28-7.32(m, 4H, Ar), 7.45(d, 4H, Ar), 7.72-7.74(m, 2H, Ar), 7.77(s, 1H, CH), 7.91-7.94(m, 2H, Ar), 8.50(d, 2H, Ar, J= 9.1 Hz); ^{13}C NMR ($CDCl_3$, 100 MHz): δ 46.7, 52.4, 76.6, 112.9, 122.6, 123.2, 123.9, 127.1, 127.8, 128.6, 134.3, 134.5, 137.6, 139.9, 142.2, 147.0, 154.1, 190.0, 191.5; LC-MS: m/z, 485 (M+1);Anal. Calcd for $C_{33}H_{28}N_2O_2$: C, 81.79; H, 5.82; N, 5.78Found: C, 81. 45; H, 5.64; N, 6.06

4.3.10. 2-(4-(4-(benzo[d][1,3]dioxol-5-ylmethyl)piperazin-1-yl)benzylidene)-1H-indene-1,3(2H)-dione (36)

Yellow solid; yield 90%; mp: 170-172^{0}C; ^{1}HNMR ($CDCl_3$, 400 MHz): δ 2.57(t, 4H, 2X CH_2, J= 4.9 Hz), 3.47-3.50(m, 6H, 3X CH_2), 5.95(s, 2H, CH_2), 6.76(s, 2H, Ar), 6.88-6.91(m, 3H, Ar), 7.72-7.74(m, 2H, Ar), 7.77(s, 1H, CH), 7.92-7.95(m, 2H, Ar), 8.50(d, 2H, Ar, J= 8.3 Hz); ^{13}C NMR ($CDCl_3$, 100 MHz): δ 46.6, 52.4, 62.5, 100.9, 107.9, 109.3, 113.0, 122.1, 122.6, 123.2, 124.0, 131.4, 134.2, 134.5, 137.6, 139.8, 142.2, 146.7, 147.0, 147.7, 154.1, 189.8, 191.4; LC-MS: m/z, 453 (M+1);Anal. Calcd for $C_{28}H_{24}N_2O_4$: C, 74.32; H, 5.35; N, 6.19Found: C, 74.53, H, 5.11; N, 5.94

4.3.11. 2-(4-(4-(pyridin-2-yl)piperazin-1-yl)benzylidene)-1H-indene-1,3(2H)-dione (37)

Yellow solid; yield 89%; mp: 178-180^{0}C; ^{1}HNMR ($CDCl_3$, 400 MHz): δ 3.64-3.67(m, 4H, 2 X CH_2), 3.75-3.77(m, 4H, 2 X CH_2), 6.66-6.69(m, 2H, Ar), 6.94(d, 2H, Ar, J= 8.4 Hz), 7.51-7.55(m, 1H, Ar), 7.73-7.75(m, 2H, Ar), 7.79(s, 1H, CH), 7.92-7.96(m, 2H, Ar), 8.21-8.22(m, 1H, Ar), 8.54(d, 2H, Ar, J= 9.1 Hz); ^{13}C NMR ($CDCl_3$, 100 MHz): δ 44.4, 46.1, 106.9, 112.9, 113.7, 122.6, 123.4, 124.2, 134.3, 134.5, 137.6, 139.8, 142.2, 146.9, 147.9, 153.8, 158.8, 189.8, 191.4; LC-MS: m/z, 396 (M+1);Anal. Calcd for $C_{25}H_{21}N_3O_2$: C, 75.93; H, 5.35; N, 10.63Found: C, 75. 61; H, 5.54; N, 10.99.

4.3.12. 2-(4-(4-(pyrimidin-2-yl) piperazin-1-yl)benzylidene)-1H-indene-1,3(2H)-dione (38)

Yellow solid; yield 91%; mp: 210-212^{0}C; ^{1}HNMR ($CDCl_3$, 400 MHz): δ 3.61(t, 4H, 2 X CH_2, J= 5.3 Hz), 4.01(t, 4H, 2 X CH2, J= 5.3 Hz), 6.56(t, 1H, Ar, J= 4.5 Hz), 6.95(d, 2H, Ar, J= 9.1 Hz), 7.73-7.76(m, 2H, Ar), 7.79(s, 1H, CH), 7.93-7.96(m, 2H, Ar), 8.34(d, 2H, Ar, J= 4.6 Hz), 8.55(d, 2H, Ar, J= 9.1 Hz); ^{13}C NMR ($CDCl_3$, 100 MHz): δ 43.0, 46.3, 110.4, 113.0, 122.6, 123.5, 124.2, 134.3, 134.6, 137.6, 139.8, 142.2, 147.0, 153.9, 157.8, 161.3, 189.8, 191.4; LC-MS: m/z, 397 (M+1);Anal. Calcd for $C_{24}H_{20}N_4O_2$: C, 72.71; H, 5.08; N, 14.13Found:C, 72. 98; H, 5.29, N, 13.92.

4.4. Biological Evaluations

4.4.1. Inhibition of AChE and BuChE

AChE and BuChE inhibitory activities of the test compounds (**27-38**) were determined by the modified Ellman's method.[27] Briefly, stock solutions of tested compounds (10 mM) were prepared in

ethanol and diluted using 0.1 M KH_2PO_4/K_2HPO_4 buffer (pH 8.0) to afford a final concentration range between (1-100 μM). Enzyme solutions were prepared by dissolving lyophilized powder in double-distilled water. The assay solution consisted of 1mL of 0.1 M phosphate buffer KH_2PO_4/K_2HPO_4, 25μL of AChE (0.22 U/mL, E.C. 3.1.1.7, from electric eel) or 25μL of BuChE (0.06 U/mL, E.C. 3.1.1.8, from equine serum) and 100 μL of various concentrations of test compounds which was allowed to stand for 5 min before 100 μL of 0.01 M DTNB were added. A positive control of donepezil was used in the same range of concentrations. The reaction was started by addition of 20μL of the 0.075 M substrate solution (acetylthiocholine/ butyrylthiocholine) and exactly 2 min after substrate addition the absorption was measured at 25°C at 412 nm. The non-enzymatic hydrolysis of acetylthiocholine/ butyrylthiocholine iodide was also measured in enzyme-free assay systems, and the results were employed as blank. In control experiments, inhibitor-free assay systems were utilized to measure the full activity. The percent inhibition was calculated by the following expression: (1-Ai/Ac) x 100, where Ai and Ac are the absorbances obtained for AChE in the presence and absence of the inhibitors, respectively, after subtracting the respective background. Each experiment was performed in triplicate, and the mean ± standard deviation was calculated. Data from concentration-inhibition experiments of the inhibitors were calculated by nonlinear regression analysis, using the Graph Pad Prism 5 program.

4.4.2. Kinetic study of AChE

Kinetic study of AChE was performed by using a previously reported method.[27] Test compound was added into the assay solution and pre-incubated with the enzyme at 37°C for 15 min, followed by the addition of substrate. Kinetic characterization of the hydrolysis of ATC catalyzed by AChE was carried out spectrometrically at 412 nm. A parallel control was made with the assay solution of no inhibitor for each time. The plots were assessed by a weighted least square analysis that assumed the variance of V to be a constant percentage of V for the entire data set. Slopes of these reciprocal plots were then plotted against the concentration of the inhibitors in a weighted analysis and K_i was determined as the ratio of the plot intercept to the plot slope.

4.4.3. Thioflavin T (ThT) assay

Commercially available peptides were first treated with hexafluoroisopropanol (HFIP) at 5mg/ml to avoid self-aggregation. The clear solution containing the dissolved peptide was then aliquoted in micro centrifuge tube. The HFIP was allowed to evaporate under a stream of nitrogen until a clear film remained in the test tube. The pre-treated $A\beta_{1-42}$ samples were then dissolved in DMSO in order to have a stable stock solution (Aβ = 1mM). For the inhibition of self-mediated $A\beta_{1-42}$ aggregation experiment, the Aβ stock solution was diluted with 50mM phosphate buffer (pH 7.4) to 25μM before use. A mixture of the peptide (10μL, 25μM, final concentration) with or without the tested compound (25μM) was incubated at 37°C for 48 h. To quantify amyloid fibril formation, the thioflavin-T fluorescence method was used.[28] Blanks containing 50 mM phosphate buffer (pH 7.4) instead of Aβ with or without inhibitors were also carried out. After incubation, samples were diluted to a final volume of 200μL with 50mM glycine–NaOH buffer (pH 8.0) containing thioflavin-T (5μM). Then, the fluorescence intensities were recorded five minutes later (excitation, 450 nm; emission, 485 nm). The percent inhibition of aggregation was calculated by the expression (1-IFi/IFc) × 100% in which IFi and IFc are the fluorescence intensities obtained for Aβ in the presence and absence of inhibitors after subtracting the background, respectively. Each measurement was run in triplicate.

4.4.4. Oxygen radical absorbance capacity (ORAC-FL) assay

The reaction was carried out in 75mM phosphate buffer (pH 7.4), and the final reaction mixture was 200μL. Antioxidant (20μL) and FL (120μL; 70mM, final concentration) solutions were placed in a black 96-well microplate (96F untreated, Nunc). The mixture was preincubated for 15 min at 37°C, and then AAPH solution (60μL, 12mM, final concentration) was added rapidly using a multichannel pipette. The microplate was immediately placed in the reader and the fluorescence recorded every minute for 80 min (excitation, 485 nm; emission, 520 nm). Samples were measured at different concentrations (1-25μM). A blank (FL + AAPH) using phosphate buffer instead of the tested compound and eight calibration solutions using Trolox (1-25μM), final concentration) as antioxidant were also carried out in each assay. A blank using phosphate buffer instead of the tested compound was also carried out. All of the reaction mixtures were prepared in triplicate, and at least three independent runs were performed for each sample. The antioxidant curves (fluorescence versus time) were normalized to the curve of the blank. The area under the fluorescence decay curve (AUC) was calculated using the following equation:

$i = 80$

$AUC = 1 + \Sigma (f_i/f_0)$

$i = 1$

Where f_0 is the initial fluorescence reading at 0 min and f_i is the fluorescence reading at time i. The net AUC was calculated by the following equation: AUC_{sample} - AUC_{blank}. The regression equations between the net AUC and the Trolox concentrations were calculated. The ORAC-FL value for each sample was calculated using the standard curve, and the ORAC-FL value of each tested compound is thus expressed as Trolox equivalents.

4.4.5. ROS measurements under H_2O_2 -induced cellular stress

ROS assay was performed in living cells as previously described by Wang and Zhu.[29] SH-SY5Y cells were seeded at 2 $x10^4$ cells per well in 96-well plates for neuroprotection activity assay. Briefly, intracellular ROS production was measured from SH-SY5Y cells by treating them with fluorescent probe 2′,7′-dichlorofluorescein diacetate (DCFH-DA) for 20 min after 24h of H_2O_2 (200µM) treatment in the presence or absence of compounds **34** and **38** (5, 10 and 20µM). As a nonpolar compound, DCFH-DA crosses cell membrane and cellular esterases cleaved diacetate groups of DCFH-DA to form non-fluorescent 2′,7′-dichlorofluorescein (DCFH). In the presence of intracellular ROS, DCFH is oxidized very quickly to highly fluorescent DCFH. The total fluorescence was measured using an ELISA plate reader (Tecan infinity 20) at an emission wavelength of 488 nm and an excitation wavelength of 524 nm.

4.4.6. TEM assay

$A\beta_{1-42}$peptide (Sigma) stock was diluted with 20mM phosphate buffer (pH 7.4) at 4°C to 40 mM before use. For the inhibition of $A\beta_{1-42}$aggregation experiment, $A\beta_{1-42}$was incubated within the presence and absence of compounds **34, 38** and curcumin at 37°C for 48h. The final concentration of $A\beta_{1-42}$ and compounds were 50µM and 25µM respectively. Aliquots (10µL) of the samples were placed on a carbon coated copper/rhodium grid for 2 min at room temperature. Each grid was stained with uranyl acetate (1%) for 2 min. The excess staining solution was removed and the specimen was transferred for imaging with transmission electron microscopy (JEOL JEM-1400).

4.4.7. Neuroprotection against H_2O_2 induced neurotoxicity

The SH-SY5Y cells were seeded in 96-well plates at a density of 2 x 10^4 per well. After 24 h of incubation, the medium was replaced with serum-free DMEM containing 200 μM H_2O_2 and different concentrations of the compounds **34** and **38** at 37ºC for 24 h. SH-SY5Y cells were cultured without test compound or H_2O_2 as control group and the results were expressed by percentage of control. Cell viability was determined using the MTT assay as described previously. Photomicrographs were also taken with the help of a camera attached to a microscope (Olympus, Japan) after 24 h of treatment to assess morphological alterations in SH-SY5Y cells.

4.4.8. Neuroprotection against $A\beta_{1-42}$ -induced neurotoxicity

$A\beta_{1-42}$ peptides were first dissolved in hexafluoroisopropanol to 1mg/ml, sonicated, incubated at room temperature for 24 h and lyophilized. The resulting $A\beta_{1-42}$ peptide film was dissolved with dimethylsulfoxide and stored at -20 °C until use. SH-SY5Y cells were harvested from flasks and plated in 96-well polystyrene plates with approximately 2 x 10^4 cells per well. Plates were incubated at 37°C for 24h to allow cells to attach. $A\beta_{1-42}$ with or without compounds (**34** and **38**) were diluted with fresh medium and added to individual wells. The plates were then incubated for an additional 48h at 37°C. Cell viability was determined using MTT assay and expressed as a percentage of control cells.

4.4.9. Cell toxicity assay

The toxic effect of compound **34** and **38** on human neuroblastoma cells (SH-SY5Y) cells was examined according to the previous method.[13-14] The SH-SY5Y cells were cultured in Dulbecco's minimum essential medium (DMEM) supplemented with 10% fetal bovine serum (FBS), 1% penicillin-streptomycin solution (10,000 units of penicillin and 10 mg of streptomycin in 0.9% NaCl) at 37°C in a humidified atmosphere containing 5% CO_2. The cells were plated in 96-well plate at a density 2000 cells/well and cultured for 24h. Next, cells were exposed to the tested compounds at different concentrations (1-100μM) for 48h. A stock solution of tested compound was prepared in DMSO and diluted in complete medium to give final concentrations. Cytotoxicity assay was performed after 48h incubation with compounds in triplicates. The MTT

reagent was added to each well for additional 4h followed by solubilisation of formazan crystals in DMSO. The absorbance of each well was measured using a microculture plate reader with a test wavelength of 570 nm and a reference wavelength of 630 nm. Results are expressed as the mean ± S.D of three independent experiments.

4.4.10. Molecular Docking studies

The X-ray crystal structures of the enzyme Torpedo californica AChE (TcAChE) (PDB ID: 1EVE) and Human BuChE (HuBuChE) (PDB ID: 4TPK)[30] were obtained from the RCSB protein data bank. Docking studies were performed using Discovery Studio (DS) Client v 4.0 package (Accelrys Inc., San Diego, CA). The ligand molecules were sketched using the Build Fragment tool in DS followed by the addition of hydrogen atoms. Valency of the ligand molecules was monitored, followed by clean geometry application. CHARMm force field was applied to the ligand followed by energy minimization using steepest descent and conjugate gradient till a derivative of 0.001 was achieved. For docking studies, initial protein was prepared by removing all water molecules, heteroatoms, any co-crystallized solvent and the ligand. Proper bonds, bond orders, hybridization and charges were assigned using protein model tools. CHARMm force field was applied using the receptor ligand interactions tool. The respective ligands were deleted and a site sphere was built to define the active site of receptor which spans the entire region. The center of the grid box was placed near the active site gorge (AChE [2.570, 64.382, 68.125, 9.533] and BuChE [132.13, 113.46, 40.88, 10.6]. The CDOCKER program DS 4.0 software was used to perform docking simulations. CDOCKER generates random conformations of ligands within the active site through high-temperature molecular dynamics to generate 10 docked ligand poses. The resultant docking orientations, within 2.0 Å in the root mean square deviation (rmsd) in tolerance of each other, were clustered together to represent the most favorable free energy of binding. Finally, the top-posed docking conformations were submitted to post-docking energy minimization on Discovery Studio 4.0. Further, the enzyme–ligand complexes were ranked based on a scoring function, CDOCKER interaction energy in kcal/mol.

In-silico Physicochemical and Pharmacokinetic analysis.

The physicochemical properties of compounds **34** and **38** were calculated by using Molinspiration online property explorer (Molinspiration Cheminformatics). The in-silico pharmacokinetic properties were calculated by using Discovery Studio 3.5 software (Accelrys, San Diego, CA, USA). The chemical structures were drawn on Chemdraw version 10 to generate the possible conformations and the obtained optimized structure was saved in Mol 2 format which was utilized for pharmacokinetic estimation.[31-33]

Acknowledgements

The author Chandra Bhushan Mishra is thankful to the University Grants Commission (UGC) for the award of Dr. D.S. Kothari postdoctoral fellowship. Authors Shikha Kumari, Apra Manral, and Vikas Saini are thankful to UGC for financial support. Manisha Tiwari is thankful to the University of Delhi for sanctioning research funds to carry out this study. University Science Instrumentation Center (USIC) is deeply acknowledged for providing NMR spectral analysis of the synthesized compounds.

References

1. Xing, W.; Fu, Y.; Shi, Z.; Lu, D.; Zhang, H.; Hu, Y. *Eur. J. Med. Chem.* **2013**,63, 95.

2. http://www.who.int/mediacentre/factsheets/fs362/en/. Accessed on March **2016**.

3. Scarpini, E.; Scheltens, P.; Feldman, H. *Lancet Neurol.* **2003**, 2, 539.

4. Pepeu, G.; Giovannini, M. G. *Curr. Alzheimer Res.* **2009**, 6, 86.

5. Hardy, J. *J. Neurochem.* **2009,** 110, 1129.

6. Nunomura, A.; Castellani, R. J.; Zhu, X.; Moreira, P. I.; Perry, G.; Smith, M. A. *J. Neuropathol. Exp. Neurol.* **2006,** 65, 631.

7. Giunta, B.; Fernandez, F.; Nikolic, W. V.; Obregon, D.; Rrapo, E.; Town, T.; Tan, J. *J. Neuroinflammation.* **2008,** 5, 5.

8. Peng, D.Y.; Sun, Q.; Zhu, X. L.; Lin, H.Y.; Chen, Q.; Yu, N. X.; Yang, W.C.; Yang, G. F. *Bioorg Med Chem*. ***2012***, 20, 6739.

9. Sun, Q.; Peng, D.Y.; Yang, S.G.; Zhu, X. L.; Yang, W.C.; Yang, G. F. *Bioorg Med Chem*. ***2014***, 22, 4784.

10. Diasa, K. S. T.; Jr, C.V. *Current Neuropharmacology*. **2014**,12, 239.

11. Peng, D.Y.; Sun, Q.; Zhu, X.-L.; Lin, H.Y.; Chen, Q.; Yu, N.-X.; Yang, W.C.; Yang, G.F. *Biorg Med Chem*. **2012**, 20, 6739.

12. Sun, Q.; Peng, D.Y.; Yang, S.G.; Zhu, X.L.; Yang, W.C.; Yang, G.F. *Biorg Med Chem.* **2014**, 22, 4784.

13. Meena, P.; Nemaysh, V.; Khatri, M.; Manral, A.; Luthra, P.M.; Tiwari, M. *Biorg .Med Chem*. **2015**, 23, 1135.

14. Manral, A.; Saini, V.; Meena, P.; Tiwari, M. *Biorg Med Chem.* **2015**, 23, 6389.

14. Giles, D.; Praksh, M. S.; Ramseshu, K.V. *E-J. Chem.* **2007,** 4, 428.

15. Inayama, S.; Mamoto, K.; Shibata, T.; Hirose, T. *J. Med. Chem.***1976**, 19, 433.

16. Shaquiquzzaman, M.; Verma, G.; Marella, A.; Akhter, M.; Akhtar, W.; Khan, M. F.; Tasneem, S.; Alam, M. M. *Eur J Med Chem*. **2015**, 102, 487.

17. Sugimoto, H.; Yamanishi, Y.; Iimura, Y.; Kawakami, Y. *Curr. Med.Chem.* **2000**, 7, 303.

18. Zhao, L. N.; Long, H. W.; Mu, Y.; Chew, L. Y. *Int. J. Mol. Sci.* **2012,** 13, 7303.

19. Hubin, E.; Nuland, N. A. J. van; Broersen, K.; Pauwels, K. *Cell. Mol. Life Sci.* **2014**, 71, 3507.

20. Sussman, J. L.; Harel, M.; Frolow, F.; Oefner, C.; Goldman, A.; Toker, L.; Silman, I. Science. **1991**, 253, 872**.**

21. Luo, W.; Chen, Y.; Wang, T.; Hong, C.; Chang, L.P.; Chang, C. C.; Yang, Y.C.; Xie, S.Q.; Wang, C. J. *Bioorg Med Chem.* **2016**, 24, 672.

22. Davalos, A.; Gomez-Cordoves, C.; Bartolome, B. *J. Agric. Food Chem*. **2003**, 51, 2512.

23. Amor, S.; Puentes, F.; Paul, D. B.; Valk van der. *Immunology.* **2010**, 129, 154.

24. Lipinski, C. A.; Lombardo, F.; Dominy, B. W.; Feeney, P. J. *Adv. Drug Delivery Rev.* **1997**, 23, 3.

25. Egan, W. J.; Merz, K. M.; Baldwin, J. J. *J. Med. Chem.* **2000**, 43, 3867.

26. Ellman, G. L.; Courtney, K. D.; Andres, V.; Feather-Stone, R. M. *Biochem. Pharmacol.* **1961**, 7, 88.

27. Naiki, H.; Higuchi, K.; Nakakuki, K.; Takeda, T. Lab. Invest. **1991**, 65, 104.

28. Wang, R.G.; Zhu, X.Z. Brain Res. **2003**, 961, 131.

29. Bolea, I.; Juárez-Jimenez, J.; de los Ríos, C.; Chioua, M.; Pouplana, R.; Luque, F. J.; Unzeta, M.; Marco-Contelles, J.A. *J. Med. Chem.* **2011**, 8251−8270.

30. Brus, B.; Košak, U.; Turk, S.; Pišlar, A.; Coquelle, N.; Kos, J.; Stojan, J.; Colletier, J.P.; Gobec, S. *J. Med. Chem.* **2014**, 57, 8167.

31. Kumari, S.; Mishra, C.B.; Tiwari, M. *Bioorg Med Chem Lett.* **2015**, 25, 1092.

32. Mishra, C.B.; Kumari, S.; Tiwari, M. *Arch Pharm Res.* **2016**, 39, 603.

33. Kumari, S.; Mishra, C.B.; Tiwari, M. *Pharmacol Rep.* **2016**, 68, 250.

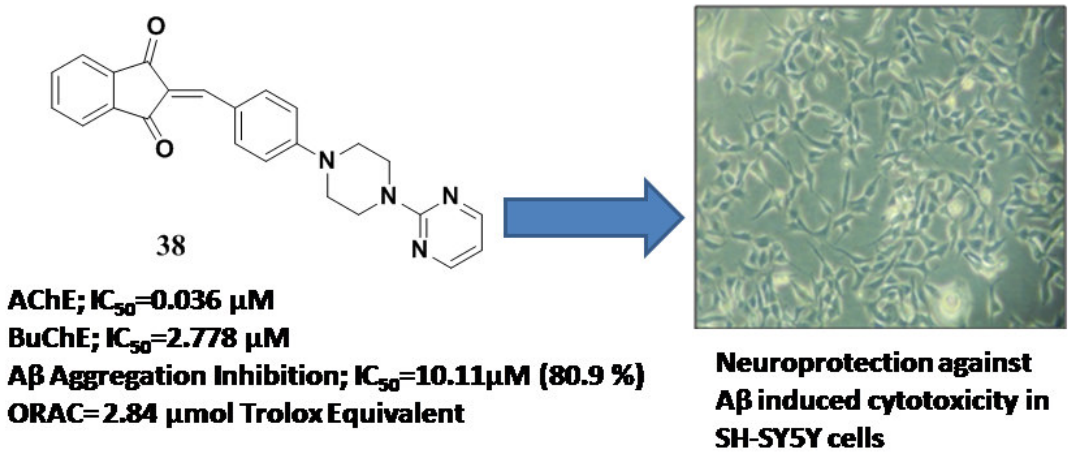

Graphical abstract

Research Highlights

- Novel Indandiones were designed and synthesized as multifunctional agents for AD.
- Most of the compounds have shown good AChE, BuChE and Aβ aggregation inhibitory activity.
- Compounds **34** and **38** appeared as most active derivative which possesses excellent AChE, BuChE and Aβ aggregation inhibition.
- Both compounds also displayed promising antioxidant activity and neuroprotection in SH-SY5Y cells.